

# Systematic study of high-K isomers in the midshell Gd and Dy nuclei

S. K. Ghorui<sup>1</sup> <sup>a</sup> and C. R. Praharaj<sup>2</sup> <sup>b</sup>

<sup>1</sup> School of Physics and Astronomy, Shanghai Jiao Tong University, Shanghai 200240, China

<sup>2</sup> Institute of Physics, Bhubaneswar-751005, INDIA

the date of receipt and acceptance should be inserted later

**Abstract.** High-K isomers are well known in the rare-earth region and provide unique access to the high spin structures of the nuclei. With the current interest in the study of neutron-rich rare-earth nuclei at Radioactive Ion Beam (RIB) facilities, we present here theoretical results of the band structures of neutron-rich Gd and Dy nuclei, including the high K-isomers. Apart from the already known K-isomers, we predict some more K-isomers and these are suggested for future studies at RIB facilities. Self-consistent Deformed Hartree-Fock and Angular Momentum Projection theories are used to get the intrinsic structures, band-spectra and electromagnetic transitions probabilities of the ground band as well as bands based on isomers.

**PACS.** 21.10.-k Properties of nuclei; nuclear energy levels, 21.60.Jz Self-consistent mean field calculations and 21.10.Ky Electromagnetic moments

## 1 Introduction

Nuclear isomers [1, 2] are excited, metastable quantum-mechanical states of nuclei. The quantum degree of freedom, K, which is the angular-momentum projection onto the symmetry axis of a deformed nucleus, is usually a good quantum number. Because of K selection rule [3], decay from a high-K state to low-K state can be hindered. Therefore, they have longer half-lives than usual excited states and form high-K isomers. K-isomeric states appear widely throughout the nuclear chart [1, 4]. Moreover, high-K isomers systematically occur in neutron-rich nuclei with  $A \geq 150$  which typically have deformed prolate shapes. Nuclear K-isomers decay predominantly by electromagnetic processes ( $\gamma$ -decay or internal conversion). There are also known instances of the decay being initiated by the strong interaction ( $\alpha$ -emission) or the weak interaction ( $\beta$ -decay or electron capture). Decay by proton or neutron emission, or even by nuclear fission, is possible for some isomers. The K-isomers serve as unique access to high-spin structure of neutron-rich nuclei. Therefore, the study of nuclear isomers, their occurrences and stability gives insight on nuclear structure of nuclei. The exploration of nuclei with isomeric states is also interesting from astrophysical point of view to understand how they affect the nucleosynthesis paths and the creation of elements heavier than Fe in the Universe [5].

The single-particle structure of nuclei in the deformed rare-earth region is still an interesting topic. In the  $A \sim 160$

mass region nuclei, high- $\Omega$  (projection quantum number on symmetry axis) orbits are available near the Fermi surfaces. Therefore, nuclei in this region are prime candidates for high-K isomers [1, 4, 6]. The decay of these high-K isomers to the ground band, which is predominantly K=0 for even-even nuclei, is hindered due to large difference in the K-values of the isomers from the ground band. The presence of isomeric states and hence their decay to low-lying states provide insight into the nuclear structure, specially collectivity in these nuclei. It has long been recognized that the nature of nuclear collectivity at low spins depends on the number of proton and neutron valence particles or holes outside the closed shells [7, 8]. Therefore, the high degree of axial symmetry and large deformation are expected for a doubly midshell nuclei. Thus one expects  $^{170}\text{Dy}$ , having large- $\Omega$  orbits near the Fermi surfaces, to be a good candidate for long-lived K-isomers. An earlier calculation [9] using the total Routhian surface (TRS) and configuration constrained potential energy surface (PES) methods predicted that pure, axially symmetric deformed shape is favored for mid-shell nuclei  $^{170}\text{Dy}$ . This is also supported by Skyrme Hartree-Fock and Projected Hartree-Fock calculations in Ref. [10]. In both the articles, a high-K isomer at low excitation energy is predicted [9, 10]. However, a recent measurement [11] shows that the  $K^\pi = 6^+$  isomer decay hindrance factor is reduced by an order of magnitude compared to the predictions. Söderström *et. al.* [11] claimed that the reduced hindrance is due to mixing with other K-configurations. Recent calculations using the triaxial projected shell model showed a strong correlation between the isomer hindrance and the properties of the  $\gamma$ -band for heavier  $N=104$  isotones [12]. In recent

<sup>a</sup> surja@sjtu.edu.cn

<sup>b</sup> crp@iopb.res.in

years many 2-qp isomers are observed experimentally for  $N=100-104$  isotones ([13,14,15,16,17] and refs. therein). Spectroscopic properties of high-K isomers in deformed nuclei with  $A > 100$  are recently evaluated by Kondev et. al. [18]. Interestingly, using isomer decay spectroscopy, Patel et. al. [15] showed the increased quadrupole collectivity near  $N=100$  for Sm and Gd nuclei as predicted in Refs. [19,20].

From astrophysical abundance pattern, apart from the prominent peaks at  $A \sim 130$  and  $A \sim 190$ , there is a small bump near  $A = 160$ . This is well-known as the rare-earth element (REE) peak. It has been suggested that the deformation plays important role in the formation of the REE peak [21]. Although, the structure of neutron-rich nuclei in the rare-earth region has broad range of interests, spectroscopic information are very limited. With the advancement of radioactive-ion beam facilities (e.g., RIBF at RIKEN) many experiments have been performed for nuclei in this mass region [15,16,11,22,23,24]. In fact, the rare-earth nuclei at  $N=100$  and beyond are candidates for study of neutron-rich nuclei at the experimental facilities [25]. Given the fact that neutron-rich nuclei are topic of current interest, it is proper to have theoretical results and predictions of deformations and possible K-isomers in this active region using microscopic models. These will further facilitate the experimental investigations. Deformed Hartree-Fock theory [26] (based on the variational principle) for intrinsic structure and Angular Momentum Projection [27] for restoration of rotational symmetry are very useful for such study.

Here we study the systematics of isomeric bands and electromagnetic properties of rare-earth nuclei employing the Deformed Hartree-Fock (DHF) and Angular Momentum ( $J$ ) projection method [26,28]. Residual interaction is included in building the deformed basis in this theory. From the self-consistent Hartree-Fock (HF) calculations, we build the intrinsic states of the bands by particle-hole excitations across the proton and neutron Fermi surfaces (the various particle-hole configurations based on HF intrinsic states), besides the Hartree-Fock configuration.  $J$ -projection from the deformed intrinsic configurations gives the spectra and electromagnetic properties of various bands [28,29]. Diagonalisation after projection can be done. This model, with the residual interaction built into the HF states, is very close to the shell model as has been shown in earlier studies [30,31].

$$\langle \psi_{K_1}^{J_1} | H | \psi_{K_2}^{J_2} \rangle = \frac{2J+1}{2} \frac{1}{(N_{K_1 K_1}^J N_{K_2 K_2}^J)^{1/2}} \int_0^\pi d\beta \sin(\beta) d_{K_1 K_2}^J(\beta) \langle \phi_{K_1} | e^{-i\beta J_y} | \phi_{K_2} \rangle \quad (3)$$

with

$$N_{K_1 K_2}^J = \frac{2J+1}{2} \int_0^\pi d\beta \sin(\beta) d_{K_1 K_2}^J(\beta) \langle \phi_{K_1} | e^{-i\beta J_y} | \phi_{K_2} \rangle \quad (4)$$

$$\langle \psi_{K_1}^{J_1} | |T^L| | \psi_{K_2}^{J_2} \rangle = \frac{1}{2} \frac{(2J_2+1)(2J_1+1)^{1/2}}{(N_{K_1 K_1}^{J_1} N_{K_2 K_2}^{J_2})^{1/2}} \sum_{\mu\nu} C_{\mu\nu K_1}^{J_2 L J_1} \int_0^\pi d\beta \sin(\beta) d_{\mu K_2}^{J_2}(\beta) \langle \phi_{K_1} | T_\nu^L e^{-i\beta J_y} | \phi_{K_2} \rangle \quad (5)$$

## 2 Deformed Hartree-Fock and Angular Momentum Projection Formalism

The present model, based on quantum many-body method, has been quite successful in explaining high spin states in the rare-earth region [19,32,33,34] and also in the lighter mass region [35,36]. In this section we briefly discuss the model used for the microscopic calculations. More details can be found in Refs. [26,28,29]. Our model consists of self-consistent deformed Hartree-Fock mean field obtained with a Surface Delta residual interaction and subsequent angular momentum projection to obtain state with good angular momentum.

The axially deformed states  $|\eta m\rangle$  are expanded in the spherical basis states as follows:

$$|\eta m\rangle = \sum_j C_{jm}^\eta |jm\rangle \quad (1)$$

where  $j$  is the angular momentum of the spherical single particle state and  $m$  its projection on symmetry axis. The mixing amplitudes  $C_{jm}^\eta$  are obtained by solving deformed Hartree-Fock equations in an iterative process (See Appendix A for more details). When the convergence in the HF solutions is obtained we get deformed single particle orbits. The residual interaction is also included self-consistently and it causes the mixing of single-particle orbits of nucleons. The deformed HF basis is enriched compared to the Nilsson basis as the  $p-p$ ,  $n-n$  and  $p-n$  correlations are built in by the inclusion of residual interaction in a self-consistent manner through the HF procedure (Eq. A 3 in the Appendix A ).

Because of mixing in the single particle orbits, the HF configurations  $|\phi_K\rangle$  are superposition of states of various  $J$  values. The states of good angular momenta can be extracted by means of projection operator [27]

$$P_K^{JM} = \frac{2J+1}{8\pi^2} \int d\Theta D_{MK}^J(\Theta)^* R(\Theta) \quad (2)$$

here  $R(\Theta)$  is the rotation operator  $e^{-i\alpha J_z} e^{-i\beta J_y} e^{-i\gamma J_z}$  and  $\Theta$  represents the Euler angles  $\alpha$ ,  $\beta$  and  $\gamma$ . The angular momentum projection operator 2 restores the rotational symmetry broken during HF procedure. By means of angular momentum projection, various high-K configurations can be described without giving any preference to the orientation of the rotation axis.

The Hamiltonian overlap between two states of angular momentum  $J$  projected from intrinsic states  $|\phi_{K_1}\rangle$  and  $|\phi_{K_2}\rangle$  is given by:

Reduced matrix elements of tensor operator  $T^L$  between projected states  $|\psi_{K_1}^{J_1}\rangle$  and  $|\psi_{K_2}^{J_2}\rangle$  are given by

where the tensor operator  $T^L$  denotes electromagnetic operators of multipolarity  $L$ .

In general, two states  $|\psi_{K_1}^{JM}\rangle$  and  $|\psi_{K_2}^{JM}\rangle$  projected from two intrinsic configurations  $|\phi_{K_1}\rangle$  and  $|\phi_{K_2}\rangle$  are not orthogonal to each other even if the intrinsic states  $|\phi_{K_1}\rangle$  and  $|\phi_{K_2}\rangle$  are orthogonal. We orthonormalise them using following equation

$$\sum_{K'} (H_{KK'}^J - E_J N_{KK'}^J) b_{K'}^J = 0 \quad (6)$$

Here  $N_{KK'}^J$  are amplitude overlap and  $b_{K'}^J$  are the orthonormalised amplitudes, which can be identified as band-mixing amplitudes. The orthonormalised states are given by

$$\Psi^{JM} = \sum_K b_K^J \psi_K^{JM} \quad (7)$$

With these orthonormalised states we can calculate matrix elements of various tensor operators. The mixing of intrinsic K structures can be deduced from the orthonormalized wave functions.

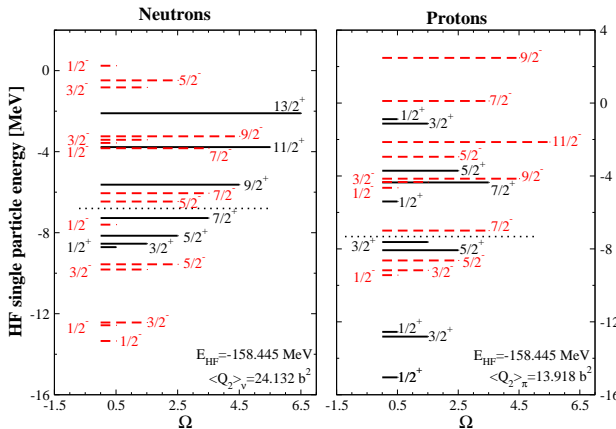


**Fig. 1.** [color online] The prolate Hartree-Fock single-particle orbits for neutrons (left panel) and protons (right panel) are shown for  $^{168}\text{Dy}$ . Solid and dashed lines correspond to the positive and negative parity orbits, respectively. The length of these lines indicate the magnitude of the z-projection ( $\Omega$ ) of the angular momentum. Dotted lines guide the eye to the Fermi levels.

### 3 Results and Discussion

In deformed (axial) Hartree-Fock and angular momentum projection (DHF) technique [for details see [28, 36] and references there in] we start with a model space and an effective interaction. The model space is presently limited to one major shell for protons and neutrons lying outside the  $^{132}\text{Sn}$  core. The  $3s_{1/2}$ ,  $2d_{3/2}$ ,  $2d_{5/2}$ ,  $1g_{7/2}$ ,  $1h_{9/2}$  and  $1h_{11/2}$  proton states have energies 3.654, 3.288, 0.731, 0.0, 6.96 and 1.705 MeV, and the  $3p_{1/2}$ ,  $3p_{3/2}$ ,  $2f_{5/2}$ ,  $2f_{7/2}$ ,  $1h_{9/2}$  and  $1i_{13/2}$  neutron states have energies 4.462, 2.974, 3.432,

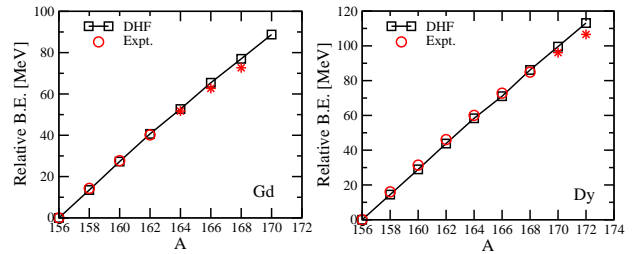


**Fig. 2.** Hartree-Fock energies of Gd (left panel) and Dy (right panel) isotopic chains calculated with DHF theory (open squares) compared with the available experimental binding energies (circles) or extrapolated values (asterisks). The calculated and experimental values are normalized w.r.t.  $A=156$ . Experimental and extrapolated data are taken from [37].

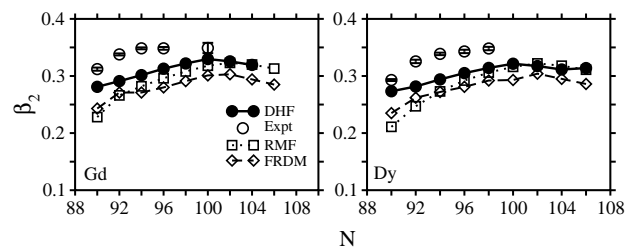


**Fig. 3.** Quadrupole deformation ( $\beta_2$ ) vs neutron number ( $N$ ) plot for Gd and Dy nuclei. Experimental data are taken from [38, 39]

0.0, 0.686 and 1.487 MeV respectively [40, 41]. The prolate HF calculation for the valence nucleons lying outside the  $^{132}\text{Sn}$  core is performed for both Gd and Dy isotopic chains presently studied. The set of prolate deformed HF orbits (with well defined  $\Omega$ -quantum numbers) shown in Fig. 1 for  $^{168}\text{Dy}$  forms the deformed single particle basis for the valence protons and neutrons. We would like to mention that the valence spaces used here, limited to one major shell each for protons and neutrons, are relatively small but adequate. Since the nuclei presently studied are lying near the middle of the shell so the shells above and below do not contribute much for the low-lying structures. Moreover, the important orbits which are responsible for low-lying high-K configurations are all included in the valence space employed here. So in that sense the present model space is adequate to describe the properties of nuclei studied here. It is worthwhile to mention that to study higher-lying structures, it would be necessary to employ a valence space consisting of more than one major shell. We use surface delta Interaction (SDI) [42] as the residual interaction among the active nucleons within the valence space. The strength of the SDI has been taken to be 0.3 MeV for  $p-p$ ,  $n-n$  and  $p-n$  interactions in our calculation [29, 32]. The strength was fixed to reproduce relative binding energies of nuclei in the rare-earth mass region [29]. In spite of its simple nature, this interaction gives a good description of the systematics of deformations in this mass region [29, 43]. Also the interaction reproduces quite well the relative experimental binding energies of the Gd and Dy isotopic chains as shown in Fig. 2.

**Table 1.** The values of HF energy ( $E_{HF}$ ), interaction energies ( $\langle V_{pp} \rangle$ ,  $\langle V_{nn} \rangle$ ,  $\langle V_{pn} \rangle$ ), the quadrupole [ $Q_2 = \langle r^2 Y_{20}(\theta) \rangle$ ] and hexadecapole [ $Q_4 = \langle r^4 Y_{40}(\theta) \rangle$ ] moments obtained for prolate Hartree-Fock ground states in  $^{164,166,168}\text{Gd}$  and  $^{166,168,170}\text{Dy}$ . The multipole moments are given in units of the harmonic oscillator length parameter,  $b = 0.9A^{1/3} + 0.7$  fm.

Z	A	$K^\pi$	$E_{HF}$ [MeV]	$\langle V_{pp} \rangle$	$\langle V_{nn} \rangle$	$\langle V_{pn} \rangle$	Q <sub>2</sub> in $b^2$		Q <sub>4</sub> in $b^4$	
				[MeV]	[MeV]	[MeV]	Proton	Neutron	Proton	Neutron
64	164	$0^+$	-130.962	-20.983	-38.154	-112.593	13.728	23.370	12.993	33.338
	166	$0^+$	-143.689	-21.016	-44.700	-121.992	13.749	23.997	12.612	14.416
	168	$0^+$	-155.287	-21.031	-49.960	-128.970	13.765	23.480	12.379	-6.388
66	166	$0^+$	-144.341	-25.418	-38.307	-123.017	13.900	23.512	9.098	30.275
	168	$0^+$	-158.445	-25.455	-44.857	-133.775	13.918	24.132	8.763	11.459
	170	$0^+$	-171.859	-25.482	-50.142	-142.538	13.930	23.596	8.433	-9.122

The nuclei studied in the present work are axially symmetric deformed nuclei and, therefore, have good K quantum number. Here we comment on the systematics of the proton/ neutron quasiparticle excitations involving large  $\Omega$  orbits (of different parities) near the respective Fermi surfaces (can be seen in Fig. 1). Such excitations are candidates for isomers, some of which have already been seen for nuclei in this region [34]. The HF orbits ( $5/2^-$ ,  $7/2^-$ ,  $9/2^-$ ) near the proton Fermi surface are built on  $h_{11/2}$  and  $h_{9/2}$  predominantly. Similarly, the HF orbits near the neutron Fermi surface are built on  $i_{13/2}$  and  $h_{11/2}$ . The orbits near the Fermi surfaces (both proton and neutron) are particularly important for K-isomers. Before going further, we want to quantify the deformation behaviour of Gd and Dy isotopic chains. This shows the ability of the present mean-field calculations in the description of general behaviour of nuclei in this mass region. As proton and neutron orbits are filled up beyond the closed-shell, the deformation increases and hence the collectivity. The maximum deformation is expected in the middle of the shell. The  $^{170}\text{Dy}$  isotope with  $Z=66$  and  $N=104$  has the largest number of valence particles for any isotope with  $A < 208$ . Hence,  $^{170}\text{Dy}$  is considered as the most collective nuclei in its ground state [9]. However, experimental data are not available at present for this isotope. In Fig. 3, we have plotted the quadrupole deformation ( $\beta_2$ ) parameters for  $N=90$  to 106 isotopes of Gd and Dy. The quadrupole and hexadecapole moments for the prolate Hartree-Fock solutions are given in Table 1. Our DHF results for  $\beta_2$  are compared with available experimental [38, 39] as well as RMF [48] and FRDM [49] calculations. All the theoretical values including DHF results are little lower than the experimental data. But the overall trends are correctly reproduced. The  $\beta_2$  values steadily increase with  $N$  and are nearly stabilized after  $N=96$  with maximum at  $N \sim 100$ . It shows that  $\beta_2$  value tends to decrease beyond  $N=102$ . From Table 1 we can see that the nuclei presently studied possess large static ground-state quadrupole moments.

The  $N=104$  marks the midshell nuclei in this mass region, therefore rotational structure with large collectivity is expected [22]. Gd and Dy nuclei near  $N=104$  are marked by large deformation for their ground band. Therefore, rotational bands are expected for these nuclei. The yrast bands are shown in Fig. 4 for  $N=100$ , 102 and 104 isotopes of Gd (a-c) and Dy (d-f). The rotational structure and level spacing of the yrast bands are well re-

produced for the experimentally known cases. The yrast and excited band structures are obtained by mixing various K-configurations (based on particle-hole excitations across the proton and neutron Fermi surfaces) with the HF ground state. In general,  $K=0$  type 2p-2h and 4p-4h excitations are important for understanding the high-spin structures. This is one way of accounting paring by preserving particle number in HF formalism. For nuclei presently studied, however, these structures and also high-K structures mix very little, reflecting the robustness of K-quantum number for axially symmetric nuclei.

K-isomers may arise from the breaking of one or more coupled nucleon pairs to form multiquasiparticle (multi-qp) states. The single particle orbits near the proton and neutron Fermi surfaces are responsible for the configuration, excitation energy and other properties of the isomers. As shown in Fig. 1, the HF orbits near the neutron Fermi surface of  $^{168}\text{Gd}$  are built on  $h_{9/2}$  and  $i_{13/2}$  orbits with admixtures from others. Excitation of a neutron from  $-5/2[512]$  to  $9/2[624]$  gives the  $K^\pi = 7^-$  intrinsic structure. Angular momentum projection (AMP) from this configuration gives the 2-qp band based on  $K^\pi = 7^-$  isomer. Similarly, the proton Fermi surface is built on  $g_{7/2}$  and  $h_{11/2}$  orbits with admixtures from others. By exciting one proton from  $-5/2[413]$  to  $7/2[523]$  one gets  $K^\pi = 6^-$  2-qp isomer. The neutron and proton 2-qp configurations are coupled to give  $K^\pi = 13^+$  4-qp structure. The high-K isomers and rotational bands based on the isomers are shown in Fig. 4. Experimental observation of these high-K isomeric band are still awaited. The dominant configurations of the isomers and their energies along with quadrupole moments as well as  $g$ -factor are listed in Table 2.

Recently, K-isomers near  $N=100$  nuclei have been observed for  $^{162,164}\text{Sm}$  [15, 16],  $^{163}\text{Eu}$  [16] and  $^{164,166}\text{Gd}$  [15, 16]. In Ref. [15], Patel *et. al.* found an enhancement of collectivity near  $Z \leq 66$ ,  $N=100$  nuclei as predicted in Refs. [19, 20]. Later, Yokoyama *et. al.* [16] also obtained similar results. The possible reason of this behaviour is the on-set deformation in these nuclei. The deformation ( $\beta_2$ ) nearly saturates after  $N=98$ .  $K^\pi = 4^-$  and  $3^+$  2-qp isomers are observed experimentally and explained well with the deformed Hartree-Fock model [16]. In the present calculations we have considered, however, isomers with  $K \geq 6$ . In  $^{164}\text{Gd}$ , we predict a  $K^\pi = 6^-$  isomer at fairly low energy, around 1.5 MeV. This isomer is based on neutron 2-qp excitation and the main configuration is

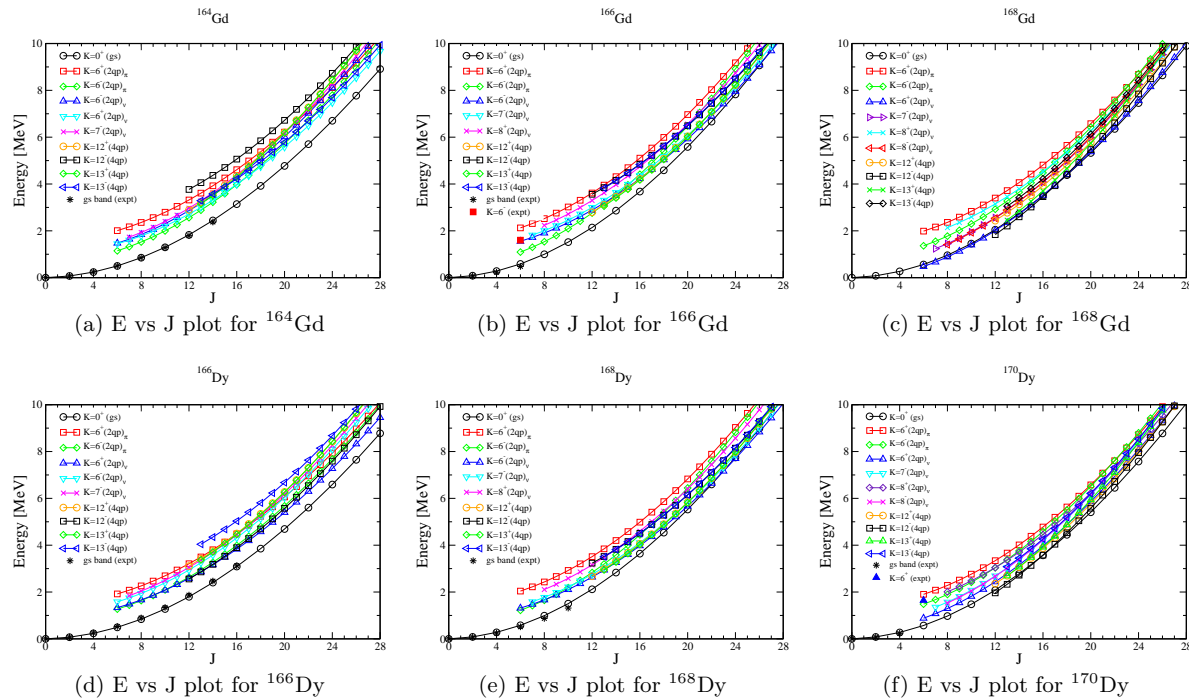


**Fig. 4.** Comparison of theoretical and experimental energy spectra. Experimental data are taken from [39, 44, 45, 46, 47].

assigned as  $\nu 5/2[512] \otimes \nu 7/2[633]$ . Two 4-qp isomers with  $K^\pi = 12^-$  are also predicted. The 4-qp isomer involving two unpaired protons ( $5/2^-$ ,  $7/2^+$ ) and two unpaired neutrons ( $5/2^+$ ,  $7/2^+$ ) is energetically favoured (with excitation energy about 2.5 MeV) compared to the other  $K^\pi = 12^-$  state which lies about 1.2 MeV higher in energy. We also predict a  $K^\pi = 12^+$  state at relatively higher excitation energy above 3.0 MeV.

A  $K^\pi = 6^-$  isomeric state at 1.288 MeV is experimentally observed for  $^{166}\text{Gd}$  [15]. This isomer has the configuration  $5/2[413] \otimes 7/2[523]$ . In DHF calculations, we obtained the isomeric state at 1.554 MeV, around 260 keV higher in energy. Our DHF results agree reasonably with the experimental value. Moreover, from the quoted  $\beta_2$  value in Ref. [15], we extracted the spectroscopic quadrupole moment ( $Q_s$ ) using the formula of Ref. [38]. The experimental extracted value, which is 4.073  $eb$  is nicely reproduced by DHF calculations (4.251  $eb$ ). A  $K^\pi = 6^-$  configuration due to proton excitation from  $-5/2^-$  to  $7/2^+$  state is obtained at 1.092 MeV. The  $K^\pi = 6^+, 7^-$  and  $8^+$  states based on proton excitations with 2-qp nature are predicted relatively higher excitation energies about 2.0 MeV. 4-qp configurations based on two proton and two neutron excitations are calculated to lie  $\approx 3.0$  MeV. All these high- $K$  configurations are listed in Table. 2.

In  $^{168}\text{Gd}$ , a 2-quasineutron isomer with configuration  $\nu 5/2[512] \otimes \nu 7/2[514]$  is obtained at very low-excitation energy  $E \approx 870$  keV. The low-excitation energy of this isomer can be understood as the neutron number increases from  $^{164}\text{Gd}$  to  $^{168}\text{Gd}$ , the  $\nu 7/2[514]$  orbital pushed down near to the neutron Fermi surface and can be easily occupied by excitations. This  $K^\pi = 6^+$  isomer possibly

have longer half-life because of large hindrance factor. Also a  $K^\pi = 7^-$  isomer from neutron excitation is predicted at 1.234 MeV. The main configuration of this isomer is  $\nu 5/2[512] \otimes \nu 9/2[624]$ . We also predict 4-qp isomers with  $K^\pi = 12^-$  (1.839 MeV),  $K^\pi = 12^+$  (2.436 MeV) and  $K^\pi = 13^+$  (2.455 MeV) at fairly low energy for this nucleus (as shown in Table 2). These 4-qp isomers are based on two unpaired neutron and two unpaired proton configurations those have low excitation energies. Therefore, 4-qp isomers also obtained with low excitation energies. As in case of Gd nuclei, 2-quasineutron  $K^\pi = 6^-$  ( $\nu 5/2[512] \otimes \nu 7/2[633]$ ) isomer is predicted for  $^{166,168}\text{Dy}$  nuclei at 1.579 MeV and 1.314 MeV, respectively. From proton excitation,  $K^\pi = 6^+$  isomer at  $E \sim 2.0$  MeV with configuration  $\pi 5/2[532] \otimes \pi 7/2[523]$  is also obtained for both N=100 and N=102 isotopes of Dy. Experimental observations of these K-isomers are awaited.

The midshell isotope  $^{170}\text{Dy}$  ( $Z=66$  and  $N=104$ ) is a very interesting candidate for low-lying isomers (both 2-qp and 4-qp). However, spectroscopic properties for the yrast band as well as excited states are extremely limited from experimental point of view. Regan *et. al.*, [9] from potential energy surface calculations predicted a  $K = 6^+$  2-quasineutron isomeric state (based on the  $5/2[512]$  and  $7/2[514]$  orbitals) at  $E \approx 1.2$  MeV in  $^{170}\text{Dy}$ . Recently, this isomer is measured experimentally and determined to have an excitation energy of  $1643.91(23)$  keV [11]. Our DHF calculations give the excitation energy of the  $K = 6^+$  isomer about  $\sim 1.0$  MeV.

The neutron orbitals  $5/2[512]$  and  $7/2[514]$  which are involved in the  $K = 6^+$  isomer are not strongly sensitive to the deformation and lie close to the Fermi surface.

**Table 2.** The dominant configuration, band-head Energy (BHE), Quadrupole moment ( $Q_S$ ) and  $g$ -factor of the isomeric configurations.

Isotope	$K^\pi$	Configuration	BHE [MeV]		$Q_S$ [eb]		$g$ -factor
			Th.	Expt.	Th.	Expt.	
$^{164}\text{Gd}$	$6^+$	$\pi 5/2[532] \otimes \pi 7/2[523]$	2.008		4.178		1.259
$^{164}\text{Gd}$	$6^-$	$\pi 5/2[532] \otimes \pi 7/2[404]$	1.146		4.278		1.007
$^{164}\text{Gd}$	$6^-$	$\nu 5/2[512] \otimes \nu 7/2[633]$	1.474		4.127		-0.126
$^{164}\text{Gd}$	$6^+$	$\nu 5/2[642] \otimes \nu 7/2[633]$	1.444		4.214		-0.144
$^{164}\text{Gd}$	$12^-$	$\{\pi 5/2[532] \otimes \pi 7/2[532]\} \oplus \{\nu 5/2[512] \otimes \nu 7/2[633]\}$	3.767		5.060		0.584
$^{164}\text{Gd}$	$12^-$	$\{\pi 5/2[532] \otimes \pi 7/2[404]\} \oplus \{\nu 5/2[642] \otimes \nu 7/2[633]\}$	2.547		5.295		0.439
$^{164}\text{Gd}$	$12^+$	$\{\pi 5/2[532] \otimes \pi 7/2[404]\} \oplus \{\nu 5/2[512] \otimes \nu 7/2[633]\}$	2.894		5.186		0.449
$^{166}\text{Gd}$	$6^+$	$\pi 5/2[532] \otimes \pi 7/2[523]$	2.126		4.228		1.267
$^{166}\text{Gd}$	$6^-$	$\pi 5/2[532] \otimes \pi 7/2[404]$	1.092		4.328		1.013
$^{166}\text{Gd}$	$6^-$	$\nu 5/2[512] \otimes \nu 7/2[633]$	1.554	1.288 <sup>a</sup>	4.251	4.073 <sup>b</sup>	-0.129
$^{166}\text{Gd}$	$7^-$	$\nu 7/2[514] \otimes \nu 7/2[633]$	1.816		4.508		0.001
$^{166}\text{Gd}$	$8^+$	$\nu 7/2[633] \otimes \nu 9/2[624]$	2.234		4.746		-0.159
$^{166}\text{Gd}$	$12^-$	$\{\pi 5/2[532] \otimes \pi 7/2[523]\} \oplus \{\nu 5/2[512] \otimes \nu 7/2[633]\}$	3.561		5.217		0.585
$^{166}\text{Gd}$	$12^+$	$\{\pi 5/2[532] \otimes \pi 7/2[404]\} \oplus \{\nu 5/2[512] \otimes \nu 7/2[633]\}$	2.794		5.342		0.448
$^{166}\text{Gd}$	$13^+$	$\{\pi 5/2[532] \otimes \pi 7/2[404]\} \oplus \{\nu 7/2[514] \otimes \nu 7/2[633]\}$	3.054		5.417		0.481
$^{168}\text{Gd}$	$6^+$	$\pi 5/2[532] \otimes \pi 7/2[523]$	1.987		4.167		1.266
$^{168}\text{Gd}$	$6^-$	$\pi 5/2[413] \otimes \pi 7/2[523]$	1.359		4.268		1.017
$^{168}\text{Gd}$	$7^-$	$\nu 5/2[512] \otimes \nu 9/2[624]$	1.234		4.524		-0.135
$^{168}\text{Gd}$	$6^+$	$\nu 5/2[512] \otimes \nu 7/2[514]$	0.866		4.234		0.053
$^{168}\text{Gd}$	$8^-$	$\nu 7/2[514] \otimes \nu 9/2[624]$	1.411		4.726		-0.017
$^{168}\text{Gd}$	$12^-$	$\{\pi 5/2[413] \otimes \pi 7/2[523]\} \oplus \{\nu 5/2[512] \otimes \nu 7/2[514]\}$	1.839		5.320		0.545
$^{168}\text{Gd}$	$12^+$	$\{\pi 5/2[532] \otimes \pi 7/2[523]\} \oplus \{\nu 5/2[512] \otimes \nu 7/2[514]\}$	2.436		5.195		0.679
$^{168}\text{Gd}$	$13^-$	$\{\pi 5/2[532] \otimes \pi 7/2[523]\} \oplus \{\nu 5/2[512] \otimes \nu 9/2[624]\}$	3.049		5.308		0.527
$^{168}\text{Gd}$	$13^+$	$\{\pi 5/2[413] \otimes \pi 7/2[523]\} \oplus \{\nu 5/2[512] \otimes \nu 9/2[624]\}$	2.455		5.435		0.402
$^{166}\text{Dy}$	$6^+$	$\pi 5/2[532] \otimes \pi 7/2[523]$	1.918		4.286		1.254
$^{166}\text{Dy}$	$6^-$	$\pi 5/2[532] \otimes \pi 7/2[404]$	1.271		4.386		1.007
$^{166}\text{Dy}$	$6^-$	$\nu 5/2[512] \otimes \nu 7/2[633]$	1.579		4.226		-0.127
$^{166}\text{Dy}$	$7^-$	$\nu 7/2[514] \otimes \nu 7/2[633]$	1.845		4.481		0.007
$^{166}\text{Dy}$	$12^-$	$\{\pi 5/2[532] \otimes \pi 7/2[523]\} \oplus \{\nu 5/2[512] \otimes \nu 7/2[633]\}$	3.775		5.184		0.582
$^{166}\text{Dy}$	$12^+$	$\{\pi 5/2[532] \otimes \pi 7/2[404]\} \oplus \{\nu 5/2[512] \otimes \nu 7/2[633]\}$	3.107		5.309		0.449
$^{166}\text{Dy}$	$13^+$	$\{\pi 5/2[532] \otimes \pi 7/2[404]\} \oplus \{\nu 7/2[514] \otimes \nu 7/2[633]\}$	3.371		5.382		0.485
$^{168}\text{Dy}$	$6^+$	$\pi 5/2[532] \otimes \pi 7/2[523]$	2.039		4.336		1.263
$^{168}\text{Dy}$	$6^-$	$\pi 5/2[532] \otimes \pi 7/2[404]$	1.218		4.436		1.014
$^{168}\text{Dy}$	$6^-$	$\nu 5/2[512] \otimes \nu 7/2[633]$	1.314		4.359		-0.130
$^{168}\text{Dy}$	$7^-$	$\nu 7/2[514] \otimes \nu 7/2[633]$	1.583		4.623		0.006
$^{168}\text{Dy}$	$8^+$	$\nu 7/2[633] \otimes \nu 9/2[624]$	2.165		4.866		-0.160
$^{168}\text{Dy}$	$12^-$	$\{\pi 5/2[532] \otimes \pi 7/2[523]\} \oplus \{\nu 5/2[512] \otimes \nu 7/2[633]\}$	3.233		5.350		0.583
$^{168}\text{Dy}$	$12^+$	$\{\pi 5/2[532] \otimes \pi 7/2[404]\} \oplus \{\nu 5/2[512] \otimes \nu 7/2[633]\}$	2.675		5.478		0.449
$^{168}\text{Dy}$	$13^+$	$\{\pi 5/2[532] \otimes \pi 7/2[404]\} \oplus \{\nu 7/2[514] \otimes \nu 7/2[633]\}$	2.942		5.554		0.485
$^{170}\text{Dy}$	$6^+$	$\pi 5/2[532] \otimes \pi 7/2[523]$	1.902		4.272		1.262
$^{170}\text{Dy}$	$6^-$	$\pi 5/2[413] \otimes \pi 7/2[523]$	1.483		4.372		1.017
$^{170}\text{Dy}$	$6^+$	$\nu 5/2[512] \otimes \nu 7/2[514]$	0.881	1.644 <sup>c</sup>	4.341		0.058
$^{170}\text{Dy}$	$7^-$	$\nu 7/2[514] \otimes \nu 7/2[633]$	1.352		4.637		-0.136
$^{170}\text{Dy}$	$8^-$	$\nu 7/2[514] \otimes \nu 9/2[624]$	1.530		4.845		-0.014
$^{170}\text{Dy}$	$8^+$	$\nu 7/2[633] \otimes \nu 9/2[624]$	2.008		4.796		-0.157
$^{170}\text{Dy}$	$12^-$	$\{\pi 5/2[413] \otimes \pi 7/2[523]\} \oplus \{\nu 5/2[512] \otimes \nu 7/2[514]\}$	1.965		5.452		0.549
$^{170}\text{Dy}$	$12^+$	$\{\pi 5/2[532] \otimes \pi 7/2[523]\} \oplus \{\nu 5/2[512] \otimes \nu 7/2[514]\}$	2.354		5.327		0.680
$^{170}\text{Dy}$	$13^-$	$\{\pi 5/2[512] \otimes \pi 7/2[523]\} \oplus \{\nu 7/2[514] \otimes \nu 7/2[633]\}$	3.076		5.442		0.525
$^{170}\text{Dy}$	$13^+$	$\{\pi 5/2[413] \otimes \pi 7/2[523]\} \oplus \{\nu 7/2[514] \otimes \nu 7/2[633]\}$	2.690		5.569		0.403

<sup>a</sup> Ref. [15]

<sup>b</sup> extracted from Ref. [15]

<sup>c</sup> Ref. [11]

face. These orbitals evolve in a similar way with deformation. It is, therefore, very unlikely that the uncertainties

in the deformation can be a dominant factor for the energy difference. Usually mixing of  $K = 0$  configurations of

$2p - 2h$  and  $4p - 4h$  paring type excitations are found to be important for the excitation energies of high-K structure. But, as shown in Table 1, the interaction energies ( $V_{pp}$ ,  $V_{nn}$  and  $V_{pn}$ ) are very large and energy gain from further mixing of other K-configurations is negligible (100 keV in this case). Also, as shown in the relative binding energy plot in Fig. 2, most of the important correlations within the present model space are already taken care of, therefore, the extension of the present configuration space may be helpful to understand the energy difference. This is beyond the scope of the present study and we plan to investigate in future.

A  $K = 6^+$  configuration involving two unpaired protons with intrinsic structure  $\pi 5/2[532] \otimes \pi 7/2[523]$  is also obtained. But this lies higher in excitation energy  $\sim 1.9$  MeV. This configuration does not mix much (<2%) with the 2-quasineutron  $K = 6^+$  configuration. Another 2-qp isomer ( $K^\pi = 7^-$ ) is identified at 1.352 MeV with configuration  $\nu 7/2[514] \otimes \nu 7/2[633]$ . We also observed 4qp isomers with  $2\pi \otimes 2\nu$  structures with excitation energy below 3.0 MeV. These isomers and their properties are given in Table 2. Some of them are predicted at low excitation energies.

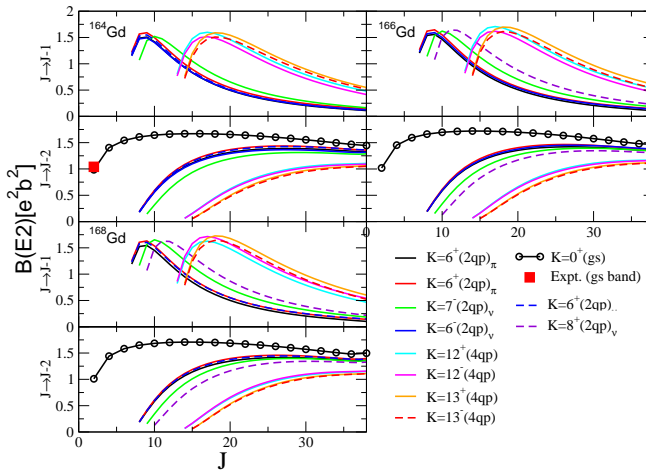


Fig. 5.  $B(E2)$  values for ground as well as 2qp and 4qp bands for  $^{164,166,168}\text{Gd}$  isotopes. Experimental data taken from Ref. [44].

For completeness, we also study the transition probabilities of the ground band as well as bands based on the isomers. Electromagnetic transition probabilities are important quantities to test the collectivity of the nuclear states. The comparison of calculated electromagnetic properties (e.g,  $B(E2)$ ,  $B(M1)$ , g-factor etc.) with experimentally available data ensures the reliability of the wave functions used to obtain them. Unfortunately, due to

experimental difficulties, information on electromagnetic properties are very scarce for the nuclei presently studied.

The  $B(E2)$  values for a transition from an initial state  $\alpha J_1$  to final state  $\beta J_2$  is given by

$$B(E2; \alpha J_1 \rightarrow \beta J_2) = \frac{1}{(2J_1 + 1)} \left| \sum_{i=p,n} \langle \Psi_{K_2}^{\beta J_2} || Q_2^i || \Psi_{K_1}^{\alpha J_1} \rangle \right|^2 \quad (8)$$

where  $i = p$  and  $n$  for protons and neutrons, respectively. The summation is for quadrupole moment operators of protons and neutrons. The  $B(E2)$  transition probabilities

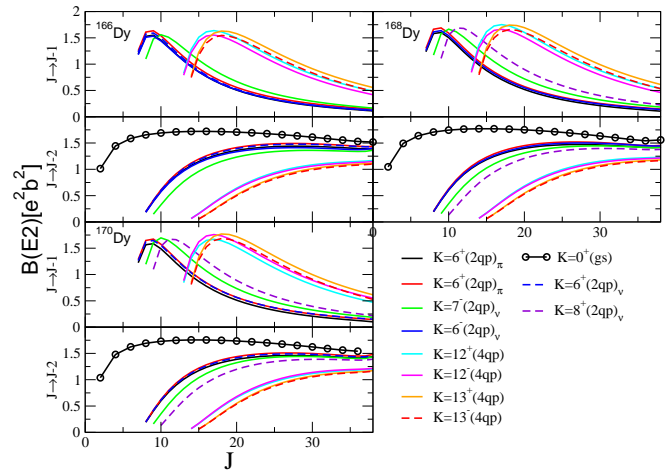


Fig. 6. Same as Fig. 5, but for  $^{166,168,170}\text{Dy}$  isotopes.

are depicted in Fig. 5 and Fig. 6 for Gd and Dy isotopes, respectively. The proton effective charges  $e_\pi = (1 + \frac{Z}{A})e$  and for the neutron  $e_\nu = (2.1 \times \frac{Z}{A})e$  are used [38]. The  $B(E2; 2_1^+ \rightarrow 0^+)$  for  $^{164}\text{Gd}$  is only known from experiment and measured to be  $198^{+11}_{-9}$  W.u. [44]. We calculate it to be 170 W.u., which compares well with the experimental value. In Figs. 5 and 6, the  $B(E2; J \rightarrow J - 2)$  values for the ground band show similar trend throughout the isotopic chains studied here. The smooth variation of transition probabilities support the rotational structure in these deformed nuclei for the ground bands.

For K-isomeric bands, in case of  $J \rightarrow J - 2$  transitions, at low-spins  $B(E2)$  values are small. The values increase with  $J$  and at high-spin become almost constant. For  $J \rightarrow J - 1$  transitions, the  $B(E2)$  values increase rapidly with  $J$  and attain a maximum value of  $\approx 1.5 e^2 b^2$  then gradually decrease. The maximum value occurs at  $J \sim 10\hbar$  for 2-qp bands and  $J \sim 18\hbar$  for 4-qp band for both Gd and Dy isotopic chains.

The reduced magnetic dipole (M1) transition moments between initial and final states are given by

$$B(M1; \alpha J_1 \rightarrow \beta J_2) = \frac{3}{4\pi(2J_1 + 1)} \left| \sum_{i=p,n} \langle \Psi_{K_2}^{\beta J_2} || g_l^i l_i + g_s^i s_i || \Psi_{K_1}^{\alpha J_1} \rangle \right|^2 \quad (9)$$

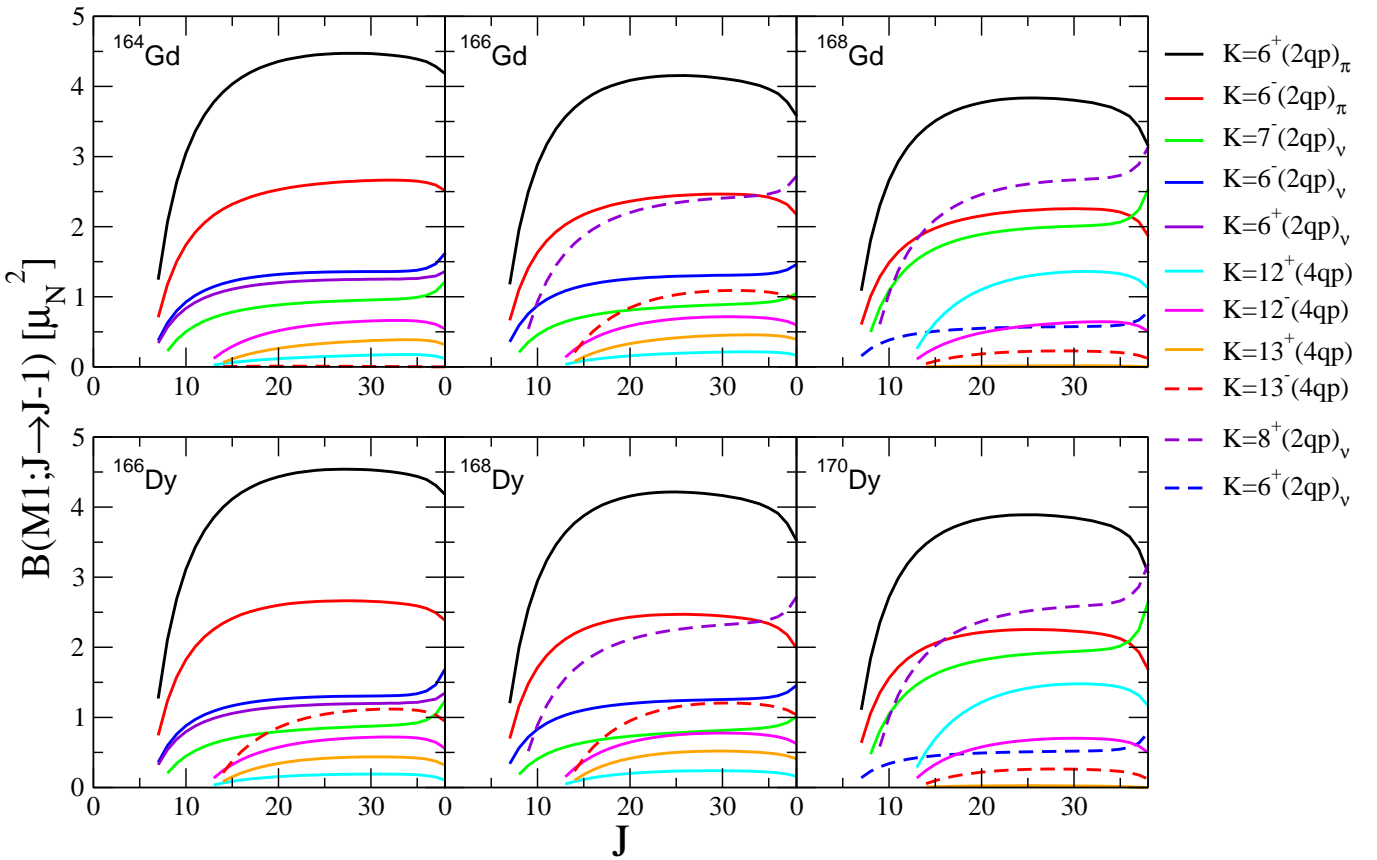


**Fig. 7.** BM1 transitions for Gd (upper panel) and Dy (lower panel) nuclei.

where  $i = p$  and  $n$  for protons and neutrons, respectively. The quantities  $g_l$  and  $g_s$  represents orbital and spin g-factors, respectively.

In Fig. 7, we have shown the  $B(M1)$  values for isomeric bands. The g-factors of  $g_l = 1.0\mu_N$  and  $g_s = 5.586 \times 0.75\mu_N$  for protons and  $g_l = 0\mu_N$  and  $g_s = -3.826 \times 0.75\mu_N$  for neutrons are used for the calculations. The quenching of spin g-factors by 0.75 is taken in account to consider the core polarization effect [50]. As these nuclei have similar deformation, therefore the bands with similar quasi-particle configuration show nearly same trends. The large M1 transition probabilities for  $K = 6^+$  band with configuration  $\pi 5/2[532] \otimes \pi 7/2[523]$  are noticeable for all nuclei studied here. Mainly the proton part contributes for this band. For most of the 4-qp bands, contribution from orbital part is negligible; proton and neutron spin parts add-up destructively (because of negative value of the neutron spin g-factor) to give a small net quantity except for  $K^\pi = 12^+$  bands in  $N=104$  isotope.

## 4 Summary

High-K isomers for the midshell Gd and Dy isotopes are studied with the self-consistent Deformed Hartree-Fock model. Angular momentum projection is performed to study bands built on the ground and excited intrinsic configurations and K-isomers. The deformation properties

of these nuclei are discussed. The  $\beta_2$  deformation varies smoothly beyond  $N=96$  with maximum around  $N=102$  for these nuclei. The known isomers are well reproduced in the present calculations. Electromagnetic properties (quadrupole moment and g-factor) of the isomers are also calculated. From the systematics, 2-qp and 4-qp isomers at low-excitation energies are predicted for these isotopes and their main-configuration as well as electromagnetic properties, which are important for experiments, are listed. These high-K isomers give unique access to the high-spin spectroscopy of *hard-to-reach* nuclei in the neutron-rich deformed rare-earth nuclei. Experimental information about high-spins for these neutron rich nuclei are very sparse and our results for the high-spins give some insight and trends. The present systematical study will further aid for the experimental quest on high-spin structure with the current generation of facilities.

## 5 Acknowledgments

Research at SJTU was supported by the National Natural Science Foundation of China (No. 11135005), by the 973 Program of China (No. 2013CB834401), and by the Open Project Program of State Key Laboratory of Theoretical Physics, Institute of Theoretical Physics, Chinese Academy of Sciences, China (No. Y5KF141CJ1). CRP acknowledges the support of the Department of Science and

Technology, Govt. of India (DST Project SB/S2/HEP-006/2013) during this work.

## References

1. P. Walker, G. Dracoulis, *Nature* **399**, 35 (1999)
2. A. Aprahamian, Y. Sun, *Nature Physics* **1**, 81 (2005)
3. A. Bohr, B. Mottelson, *Nuclear structure, Volume II*, Nuclear Structure (World Scientific, 1975), ISBN 9789810239794
4. P.M. Walker, F.R. Xu, *Physica Scripta* **91**, 013010 (2016)
5. E.M. Burbidge, G.R. Burbidge, W.A. Fowler, F. Hoyle, *Reviews of Modern Physics* **29**, 547 (1957)
6. G.D. Dracoulis, P.M. Walker, F.G. Kondev, *Reports on Progress in Physics* **79**, 076301 (2016)
7. R.F. Casten, D.D. Warner, D.S. Brenner, R.L. Gill, *Phys. Rev. Lett.* **47**, 1433 (1981)
8. R.F. Casten, N.V. Zamfir, *Phys. Rev. Lett.* **70**, 402 (1993)
9. P.H. Regan, F.R. Xu, P.M. Walker, M. Oi, A.K. Rath, P.D. Stevenson, *Physical Review C* **65**, 037302 (2002)
10. A.K. Rath, P.D. Stevenson, P.H. Regan, F.R. Xu, P.M. Walker, *Phys. Rev. C* **68**, 044315 (2003)
11. P.A. Söderström, P.M. Walker, J. Wu, H.L. Liu, P.H. Regan, H. Watanabe, P. Doornenbal, Z. Korkulu, P. Lee, J.J. Liu et al., *Physics Letters B* **762**, 404 (2016)
12. F.Q. Chen, Y. Sun, P.M. Walker, G.D. Dracoulis, Y.R. Shimizu, J.A. Sheikh, *Journal of Physics G: Nuclear and Particle Physics* **40**, 015101 (2013)
13. G.S. Simpson, W. Urban, J. Genevey, R. Orlandi, J.A. Pinston, A. Scherillo, A.G. Smith, J.F. Smith, I. Ahmad, J.P. Greene, *Phys. Rev. C* **80**, 024304 (2009)
14. E.H. Wang, J.H. Hamilton, A.V. Ramayya, J.K. Hwang, S.H. Liu, N.T. Brewer, Y.X. Luo, J.O. Rasmussen, S.J. Zhu, G.M. Ter-Akopian et al., *Phys. Rev. C* **90**, 067306 (2014)
15. Z. Patel, P.A. Söderström, Z. Podolyák, P. Regan, P. Walker, H. Watanabe, E. Ideguchi, G. Simpson, H. Liu, S. Nishimura et al., *Physical Review Letters* **113**, 262502 (2014)
16. R. Yokoyama, S. Go, D. Kameda, T. Kubo, N. Inabe, N. Fukuda, H. Takeda, H. Suzuki, K. Yoshida, K. Kusaka et al., *Physical Review C* **95**, 034313 (2017)
17. E. Ideguchi, G.S. Simpson, R. Yokoyama, M. Tanaka, S. Nishimura, P. Doornenbal, G. Lorusso, P.A. Söderström, T. Sumikama, J. Wu et al., *Phys. Rev. C* **94**, 064322 (2016)
18. F. Kondev, G. Dracoulis, T. Kibédi, *Atomic Data and Nuclear Data Tables* **103-104**, 50 (2015)
19. S.K. Ghorui, B.B. Sahu, C.R. Praharaj, S.K. Patra, *Physical Review C* **85**, 064327 (2012)
20. L. Satpathy, S. Patra, *Nuclear Physics A* **722**, C24 (2003)
21. R. Surman, J. Engel, J.R. Bennett, B.S. Meyer, *Phys. Rev. Lett.* **79**, 1809 (1997)
22. P.A. Söderström, J. Nyberg, P.H. Regan, A. Algora, G. de Angelis, S.F. Ashley, S. Aydin, D. Bazzacco, R.J. Casperson, W.N. Catford et al., *Phys. Rev. C* **81**, 034310 (2010)
23. L. Gurgi, P. Regan, P.A. Söderström, H. Watanabe, P. Walker, Z. Podolyák, S. Nishimura, T. Berry, P. Doornenbal, G. Lorusso et al., *Radiation Physics and Chemistry* **140**, 493 (2017)
24. H. Watanabe, G. Zhang, K. Yoshida, P. Walker, J. Liu, J. Wu, P. Regan, P.A. Söderström, H. Kanaoka, Z. Korkulu et al., *Physics Letters B* **760**, 641 (2016)
25. R. Yokoyama, private communication
26. G. Ripka, *The Hartree-Fock Theory of Deformed Light Nuclei*, in *Advances in Nuclear Physics*, edited by M. Baranger, E. Vogt (Plenum, 1966), Vol. 1 of *Advances in Nuclear Physics*, pp. 183–259
27. R.E. Peierls, J. Yoccoz, *Proceedings of the Physical Society A* **70**, 381 (1957)
28. C.R. Praharaj, *Physics Letters B* **119**, 17 (1982)
29. S.K. Ghorui, P.K. Raina, P.K. Rath, A.K. Singh, Z. Naik, S.K. Patra, C.R. Praharaj, *Int. J. Mod. Phys. E* **21**, 1250070 (2012), 1106.3152
30. M. Macfarlane, A. Shukla, *Physics Letters B* **35**, 11 (1971)
31. S.B. Khadkikar, S.C.K. Nair, S.P. Pandya, *Physics Letters B* **36**, 290 (1971)
32. A.K. Rath, C.R. Praharaj, S.B. Khadkikar, *Phys. Rev. C* **47**, 1990 (1993)
33. Z. Naik, C.R. Praharaj, *Phys. Rev. C* **67**, 054318 (2003)
34. S.K. Ghorui, C.R. Praharaj, P.K. Raina, Z. Naik, S.K. Patra, *AIP Conference Proceedings* **1609**, 135 (2014)
35. C.R. Praharaj, *Journal of Physics G Nuclear Physics* **14**, 843 (1988)
36. S.K. Ghorui, P.K. Raina, A.K. Singh, P.K. Rath, C.R. Praharaj, *ArXiv e-prints* (2011), 1111.1174
37. M. Wang, G. Audi, F. Kondev, W. Huang, S. Naimi, X. Xu, *Chinese Physics C* **41**, 030003 (2017)
38. S. Raman, C.W.G. Nestor, Jr, P. Tikkanen, *Atom. Data Nucl. Data Tabl.* **78**, 1 (2001)
39. *ENSDF Database*, <http://www.nndc.bnl.gov/ensdf>
40. A. Bohr, B. Mottelson, *Nuclear Structure, Volume II, page 222-223*, Nuclear Structure (World Scientific, 1975), ISBN 9789810239794
41. S. Kahana, H.C. Lee, C.K. Scott, *Phys. Rev.* **180**, 956 (1969)
42. A. Faessler, A. Plastino, S.A. Moszkowski, *Phys. Rev.* **156**, 1064 (1967)
43. C.R. Praharaj, S.K. Patra, R.K. Bhowmik, Z. Naik, J. of Phys.: Conf. Seri. **312**, 092052 (2011)
44. B. Singh, J. Chen, *Nuclear Data Sheets* **147**, 1 (2018)
45. C.M. Baglin, *Nuclear Data Sheets* **109**, 1103 (2008)
46. C.M. Baglin, *Nuclear Data Sheets* **111**, 1807 (2010)
47. C.M. Baglin, *Nuclear Data Sheets* **96**, 611 (2002)
48. G.A. Lalazissis, S. Raman, P. Ring, *Atom. Data Nucl. Data Tabl.* **71**, 1 (1999)
49. P. Möller, J.R. Nix, W.D. Myers, W.J. Swiatecki, *Atomic Data and Nuclear Data Tables* **59**, 185 (1995), nucl-th/9308022
50. B. Castel, I. Towner, *Modern Theories of Nuclear Moments*, Oxford studies in nuclear physics (Clarendon Press, 1990), ISBN 9780198517283

## A Deformed Hartree-Fock equation with axial symmetry

The configuration generated in deformed Hartree-Fock theory are obtained after self-consistent calculation including the effect of the residual interaction. The Hamiltonian is

$$H = H_0 + V, \quad (\text{A } 1)$$

where,  $H_0$  obtained from the single particle energies of protons and neutrons  $H_0 = \sum_{jm} \varepsilon_j a_{jm}^\dagger a_{jm}$ .  $V$  is the residual interactions among valance nucleons  $V_{pp}$ ,  $V_{pn}$  and  $V_{nn}$ . The matrix elements of  $V$ 's are suitably antisymmetrized for  $V_{pp}$  and  $V_{nn}$ .

With axial-symmetry of the Hartree-Fock (HF) field a HF nucleon orbit  $|\eta m\rangle$  is a superposition of spherical orbits:

$$|\eta m\rangle = \sum_j C_{jm}^\eta |jm\rangle \quad (\text{A } 2)$$

where  $j$  is the angular momentum of the shell model single particle states and  $m$  its projection. The amplitude  $C_{jm}^\eta$  of the spherical state  $|jm\rangle$  in the orbit  $\eta$  obtained by solving the deformed Hartree-Fock equations

$$E^\eta C_{jm}^\eta = \varepsilon_j C_{jm}^\eta + \sum V(j_1 m j_2 m_2; j m j_4 m_2) \rho_{j_2 m_2 j_4 m_2} C_{j_1 m}^\eta \quad (\text{A } 3)$$

where  $\varepsilon_j$  the single-particle energy of shell model orbit  $j$  ( $\equiv nlj$ ),  $V$  denotes the two-body interaction among nucleons and  $\rho$  is the density matrix

$$\rho_{j_1 m j_2 m} = \sum_{\text{occupied}} C_{j_1 m}^{\eta *} C_{j_2 m}^\eta \quad (\text{A } 4)$$

Eqns. A 3 and A 4 are solved by iteration process till there is convergence, by diagonalizing the HF Hamiltonian  $h = \varepsilon + V\rho = \varepsilon + \Gamma$  in each iteration.  $\Gamma = V\rho$  is the HF self-energy.

All intrinsic quantities follow from the density matrix  $\rho$  of the HF calculation. For example,

$$\langle Q_{20} \rangle_{HF} = \text{Tr}(Q_{20}\rho) \quad (\text{A } 5)$$

So deformation is not something externally imposed. It follows dynamically from the HF theory. Of course, the intrinsic states are not the physical states. One needs angular momentum projection from the intrinsic states to obtain the physical states with good angular momentum.

The effects of residual interaction  $V$  is taken into account at each iteration of the HF procedure (Eqns. A 3 and A 4) and it plays important role in determining the mixing amplitudes in the HF process. Essentially each HF configuration shows the intrinsic distribution of the valence nucleons in the deformed shell model orbits. It is found that angular-momentum projection from a few low-lying HF configurations gives a reasonable description of the yrast structure. This is due to the fact that the residual interaction has been used in the solution of the HF equations, so that the HF single-particle states and the various multi-particle configurations built from them are already closer to the final answer that comes from a full solution of the many-body Schrödinger equation [30, 31]. In fact angular momentum projection from a single K-configuration reproduces the energy features of the low-lying yrast states with good accuracy. Therefore, further elaborate configuration mixing (band-mixing) is not necessary.